NUMERICAL SIMULATION OF HEAT TREATMENT OF Ti-6Al-4V BY USING A PHASE-FIELD METHOD BASED SOFTWARE

Johann P. Mogeritsch, Andreas Ludwig – Montanuniversität Leoben, Austria
Gerhard Panzl, Alexander Walzl, –DISTech, Austria

ABSTRACT

Ti-6Al-4V is common material for additive manufacturing. However, parts formed by Selected Laser Melting are known to be brittle so that a post-process heat treatment is required. One important goal for this additional production step is the degeneration of the martensitic α´-phase that had formed by the extreme conditions during layer-wise production. By using a phase-field based software that couples thermodynamic information with a diffusion solver to get a spatially resolved phase transformation description, we have investigated the microstructural dynamic of heat treatment procedures typical for additive manufactured Ti-6Al-4V parts. The model describes modification of the grain sizes and shapes, evolution of phases, and corresponding concentration distributions during phase transition induced by annealing.

KEYWORDS

Ti-6Al-4V, additive manufacturing, phase-field method, heat treatment; titanium alloys; phase transformation.

INTRODUCTION

Selective Laser Melting (SLM) is an additive manufacturing process in which a laser with high power density is used to fuse a metal powder into a solid material-component [1]. Fusing layer by layer via melting and solidifying, a near-net-shape three-dimensional component with highly complex geometric features can be produced. In principle, any weldable metal alloy can be processed with SLM. High-strength properties in combination with high-temperature capability make titanium alloys particularly interesting for applications in engine- and turbine components in the aerospace industry. Titanium (Ti) has a desirable combination of high specific strength, excellent corrosion resistance, and fracture resistance. Ti is often alloyed with various alloying elements [2] to achieve a certain performance. For example, to reach high strength and good formability, aluminum (Al) and vanadium (V) are added to form Ti64, a pre-alloyed Ti-6Al-4V powder. An alloy used for hip implants that are particularly sought-after in medical technology [3-5].

In general, the element Ti consists of two main crystallographic forms, the low temperature hexagonal close-packing α-phase (hcp) and the high temperature body centered cubic β-phase (bcc). Martensitic α' forms upon fast cooling from temperatures above the critical temperature T_c. The critical temperature is defined as the temperature above which martensitic α´ forms upon water or air cooling. The temperature has been estimated in [6,7] and was found to be between 1145 K and 1166 K. The gained "as -built" microstructure in SLM consists of martensitic α´-Ti due to the highly localized heat input and short interaction time by the laser beam, large temperature gradients, and high cooling rates [8, 9]. The martensitic microstructure is undesirable since it reduces the deformability of the created component. The formability of Ti alloys is characterized by the ratio between lamellar and equiaxed grains, the grain size, and the ratio between the α-phase and the β-phase [5]. Lamellar structures increase fracture toughness and resistance against creep and crack propagation. Equiaxed structures have high fatigue strength and elongation at fracture, suitable for plastic defor-

mation. Bimodal microstructures are formed by a combination of lamellar and globular microstructure and ensure a balanced mechanical behavior.

For the α-phase microstructure, a thermomechanical process (TMP) enables grain fragmentation and globularisation [10]. First, the microstructural morphology is adapted by using hot forming to induce dislocations. Here, equiaxed grains are formed at the grain boundaries due to the preferred globularisation. Finally, a second annealing is applied to relieve residual stresses. The challenge in achieving a bimodal microstructure by post-processing SLM produced Ti-6Al-4V alloys is that the initial microstructure consists of martensitic α´-Ti instead of the hcp α-phase. [11] investigated the mechanism of grain morphology transformation in the solid solution temperature range as a function of annealing temperature, holding time, and quenching of SLM-produced martensitic α´-Ti. It was shown that a bimodal microstructure in SLM-produced Ti-6Al-4V is possible without thermomechanical treatment. Microstructures consisting of fragmented equiaxed primary α-grains in a matrix of α- plus β-lamellae can be achieved by different quenching rates from above 1173 K ($>T_c$), followed by an annealing below 1073 K [11].

In this work, the effect on the Ti-6Al-4V microstructures by heat treatment was investigated based on the experimental investigations done by [11]. The numerical experiments were carried out by using the phase field-based software program MICRESS 6.2 [12] in combination with different published diffusion coefficients for α/β-Ti. To perform aging heat treatment, the sample was annealed and quenched, whereby, the annealing times, temperatures, and quenching rates were varied.

METHOD

In this chapter we describe (i) the challenges for a phase-field based approach to deal with martensite and our assumptions, (ii) the selection of the diffusion coefficients, (iii), the definition of the domain, and (iv) the selected numerical and physical parameters.

(i) Martensitic structures are a challenge for any phase field method. Martensite is not an equilibrium phase and as such is it neither compatible to the CALPHAD approach of thermodynamic database assessment nor to the local (quasi-) equilibrium assumption of the phase field-based code. Furthermore, the martensitic configuration is a displacement process, and thus, there are no phase boundaries that move to achieve equilibrium. To nevertheless handle the phase evolution of fully martensitic α` microstructures during aging heat treatment, we assume that α` behaves thermodynamically like α. So, the reader should keep in mind that in this work the terminus α-phase means that the phase α may consists of α and an unknown amount of α`. Note that the objective of this work is not to finally estimate the remaining amount of α`. However, we start our phase field simulations with a predefined “as-built” microstructure that mimics experimental findings published by Ter Haar et al. [11]. So, we start with a 100% martensitic microstructure with consists of α`-grains that can be classified into four size classes. The subsequent diffusion-driven motion of phase boundaries, including β-phase nucleation, is then calculated based on thermodynamic information of the equilibrium α- and β- phases.

The advantage of the phase field method is that it can describe the phase evolution in 2D or 3D by coupling a diffusion solver with CALPHAD data. Fig. 1 shows a CALPHAD-based estimation of the amount of phase fractions as function of temperature for a Ti-6Al-4V alloy. The β-transus temperature is at 1215 K. The corresponding α phase amount for the two examined annealing temperatures correspond to 0.7 for 1023 K and 0.38 for 1143 K as shown as red lines in Fig. 1.

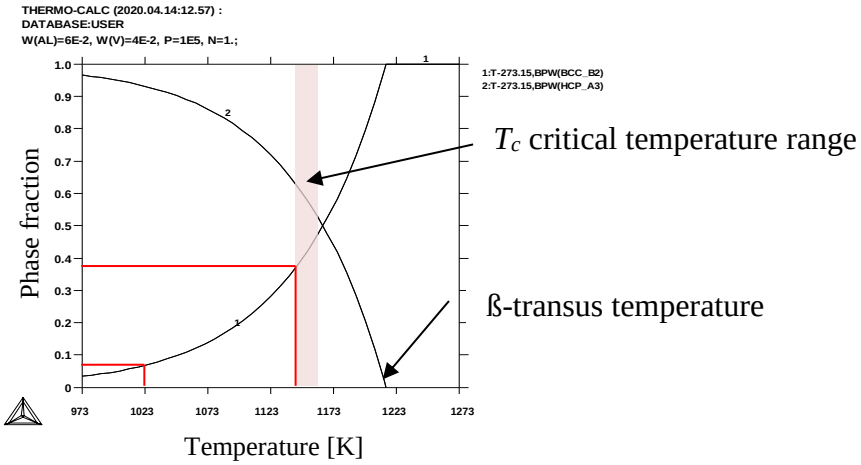

Fig. 1: Calculated phase fraction with Thermo-Calc by using the data bank Cost2 [13].

(ii) The microstructural alteration is controlled by the thermally activated process of diffusion. Therefore, the knowledge of the pre-exponential diffusion factor D_o and the diffusion activation energy Q is a prerequisite for the numerical investigations to determine the dynamic of the microstructure alteration during heat treatment. The diffusion of various alloying elements for β-Ti has been extensively observed by [14, 15]. For α-Ti, numerous difficulties in the experiment such as specimen purity, availability of tracer elements, and surface oxidation hinder the estimation of diffusion coefficients [15, 16]. Furthermore, for both phases varied experimental studies and calculation methods were used. Hence, the resulting coefficients depend on the accuracy of the experimental diffusion data as well as the assumption of the used calculation models. Xu et al. [14] carried out a computer-aided and data-driven investigation of the diffusion of dissolved substances in Ti alloys and summarizes the general trends for the diffusion of alloy elements in α-Ti in particular $D_{Ti\text{-}V} > D_{Ti} > D_{Ti\text{-}Al}$. Lindwall et al.[17] studied the diffusion in the T-Al-V system with CALPHAD [18] und determined the V diffusion coefficient between $1{\cdot}10^{-10}$ cm^2/s at 1073 K and $1{\cdot}10^{-8}$ cm^2/s at 1473 K. For Al, the coefficient was specific with $1{\cdot}10^{-9}$ cm^2/s at 1223 K. The published values are shown in Table 1. The selected values for the numerical investigations are given in Table 2 at the end of this section. If values exist parallel or normal to the crystallographic plane the average value was taken in the present study.

Table 1: Published Diffusion coefficients

Element	Phase	$D_{o\perp}$	$D_{o//}$	$Q_\perp$	$Q_{//}$
		cm^2/s	cm^2/s	J/mol	J/mol
Al [14]	α	$8.0{\cdot}10^{-2}$	$9.59{\cdot}10^{-2}$	$3.7{\cdot}10^{5}$	$3.2{\cdot}10^{5}$
Al [19]	α	$1.034{\cdot}10^{-2}$	$0.929{\cdot}10^{-2}$	$2.6{\cdot}10^{5}$	$2.6{\cdot}10^{5}$
Al [20]	α	$1.4{\cdot}10^{-2}$		$3.26{\cdot}10^{5}$	
Al [16]	α	$6.6{\cdot}10^{-1}$		$3.3{\cdot}10^{5}$	
V [14]	α	$8.99{\cdot}10^{-2}$	$8.79{\cdot}10^{-2}$	$2.6{\cdot}10^{5}$	$2.6{\cdot}10^{5}$
Al [21]	β	$5.3{\cdot}10^{-2}$		$2.2{\cdot}10^{5}$	
V [17]	α, β	$1.19{\cdot}10^{1}$		$2.5{\cdot}10^{5}$	

(iii) The object of the simulations was describe the solid-solid transformation and grain alteration below the β-transus temperature during aging heat treatment of Ti-6Al-4V. The numerical domain should reflect the characteristic properties of martensitic microstructures. Moreover, it is important to ensure that the essential mechanisms occurring during heat treatment can be reproduced within

an acceptable calculation time. To meet these conditions, the "as-built" microstructure was selected to reveal an adequate selection of grain shapes and grain sizes. According to [11] the “as-built” martensitic microstructure consisted of 4 different classes of needle-like grains. The size of the grains reached from grains with more than 20 µm length and 3 µm width (first class), down to the grains smaller than 2 µm with a width of less than 10 nm (forth class). To display one primary grain with a length of 20 µm and the associated amount of quaternary grains with less than 10 nm width in a single domain, its size should be at least 20 µm with grid size of 10 nm or less. As shown in [11] the length of the secondary grains correspond to the length of the primary grains and they are almost at right angles to each other. A reproduction of this microstructure pattern would require around 2000 x 2000 cells with a grid size of 10 nm. Due to the shape of the quaternary grains of less than 2µm x 10 nm, more than 16000 grains and corresponding grain boundaries would be represented in such a domain. Although theoretically possible, we have decided to slightly simplify the predefined “as-built” microstructure such that the computation time become manageable.

First, a lookup table with 500 x 200 entries was put together where each entry was define as either martensitic α´-phase or grain boundary such that the needle-like martensite structure and the specific widths between 10 nm and 3 µm of the four different grain classes, primary, secondary, ternary, and quaternary, as given by [11] was approximately reproduced.

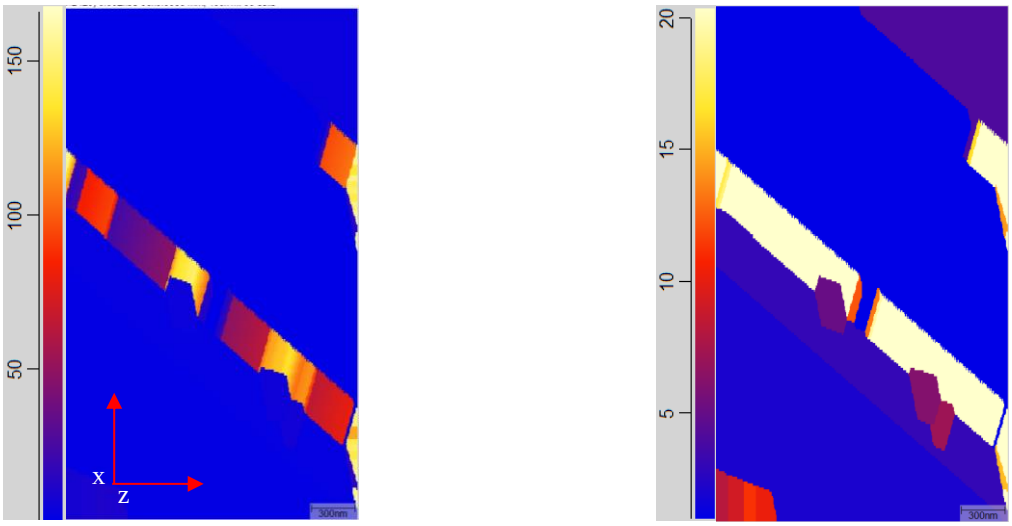

(a) (b)

Fig. 2: The predefined microstructure with four different grain classes and a total of 166 different grains. All grains are displayed in different colors. (a) The multicolored bands in the center and in the upper right represent the huge amount of quaternary grains. (b) The same microstructure with a color display for only the largest 20 grains. So the primary (dark blue) and secondary grains (violet) are optically distinguishable. The colored area in the lower left corner represents the ternary grains.

Next, the lookup table was automatic adopted to a selected rectangular domain with 2×3.5 µm^2 in size consisting of 400 cells in the *X*-direction and 700 cells in *Z*-direction (see Fig. 2.) This gave a total of 280.000 cells of 5x5 nm^2 in size. The selected cell size and number of cells enabled an acceptable simulation time and quantitative statements about the dynamic of the microstructure evolution during aging heat treatment.

(iv) For the nucleation of the β-phase we have applied the “Undercooling” model of MICRESS [12]. The model considers nucleation at a certain undercooling compare to the β-transus temperature and sets randomly as many nuclei of a critical size as possible at the grain boundaries, whereby, a predefined minimum distance of 0.1 µm between the nuclei was set to avoid clustering. The criti-

cal size for the nucleus was set to 5.5 nm to overcome the numerical undercooling governed by the grid size of 5 nm. The selected annealing temperatures and times were taken from [11] and the cooling rates from [19]. The boundary conditions at the domain walls were set as "symmetric" to represent an infinite domain size. The corresponding physical and numerical parameters that were used for the numerical simulation are given in Table 2.

Table 2**:** Numerical and physical parameter used within this work.

Names	Symbol	Unit	Value
surface energy, α-phase	$\sigma_{s/l,\alpha}$	J/cm^2	$2.0\cdot10^{-5}$
surface energy, β-phase	$\sigma_{s/l,\beta}$	J/cm^2	$2.0\cdot10^{-5}$
annealing temperatures	T	K	1023 and 1143
cooling down rates	$\dot{T}$	K/s	0.7 and 0.18
annealing times	t	s	14400, 10800, and 28800
kinetic coefficient, α-phase	μ_α	cm^4/J·s	$5\cdot10^{-10}$
kinetic coefficient, β-phase	μ_β	cm^4/J·s	$5\cdot10^{-10}$
kinetic coefficient, α/β-phase	$\mu_{\alpha/\beta}$	cm^4/J·s	$5\cdot10^{-10}$
Al, diffusion coefficient, α-phase	$D_{o,Al,\alpha}$	cm^2/s	$8.8\cdot10^{-2}$
Al, activation energy, α-phase	$Q_{,Al,\alpha}$	J/mol	$3.45\cdot10^{5}$
Al, diffusion coefficient, β-phase	$D_{o,Al,\beta}$	cm^2/s	$5.3\cdot10^{-2}$
Al, activation energy, β-phase	$Q_{,Al,\beta}$	J/mol	$2.2\cdot10^{5}$
V diffusion coefficient, α-phase	$D_{o,V,\alpha}$	cm^2/s	$8.8\cdot10^{-2}$
V activation energy, α-phase	$Q_{,V,\alpha}$	J/mol	$2.6\cdot10^{5}$
V, diffusion coefficient, β-phase	$D_{o,V,\beta}$	cm^2/s	$1.19\cdot10^{1}$
V, activation energy, β-phase	$Q_{,V,\beta}$	J/mol	$2.5\cdot10^{5}$

RESULTS AND DISCUSSION

This section outlines the obtained numerical results, including phase transitions, modification of the grain sizes, concentration distributions, and evolution of the phase fractions during heat treatment. Note that as mentioned before the phase field code cannot distinguish between martensitic α` and equilibrium α-phase. For the following interpretation of the results, we referee to α as a phase that behaves thermodynamically as α but may consist of α plus an unknown amount of α`.

Fig. 3a gives the initial situation at t = 0 s which was assumed to be identical for all numerical investigations. Of course, the microstructure consists at the beginning solely of martensitic α`-Ti (displayed in orange color) and grain boundaries (visible by the blue lines). Different areas of the original microstructure have been numbered to facilitate the description within the text. The dynamic of the microstructure evolution at an annealing temperature of 1023 K is given in Fig. 3b-e. The temperature was hold for 8 hours and then the sample was quenched to 293 K (= RT) with a cooling rate of $\dot{T}$ = 0.7 K/s.

Within the first hour the quaternary grains disappeared. This is identifiable by the erasement of the fine blue lines that indicate clusters of quaternary grain boundaries (marked as region 4 in Fig. 3a). Also within the first hour the β-phase nucleated at the grain boundaries on several locations (visible as white dots in Fig. 3b). Note that during quenching, the ß-phase should transformed back into the α-phase (see Fig. 3j). However, in our simulations the β-phase did not completely disappear: individual numerical cells had still β-fraction less than 0.7. These cells were not explicitly indicted, they

were depictured similar to the grain boundaries cells. Fig. 3b-h show that the ternary grains (marked as region 3 in Fig. 3a) began to unify. In contrast, the primary grain (labeled with 1) broadened at the cost of the ternary grains (region 2). Thereby, the secondary and the ternary grains (labelled with 2 and 3) were becoming smaller.

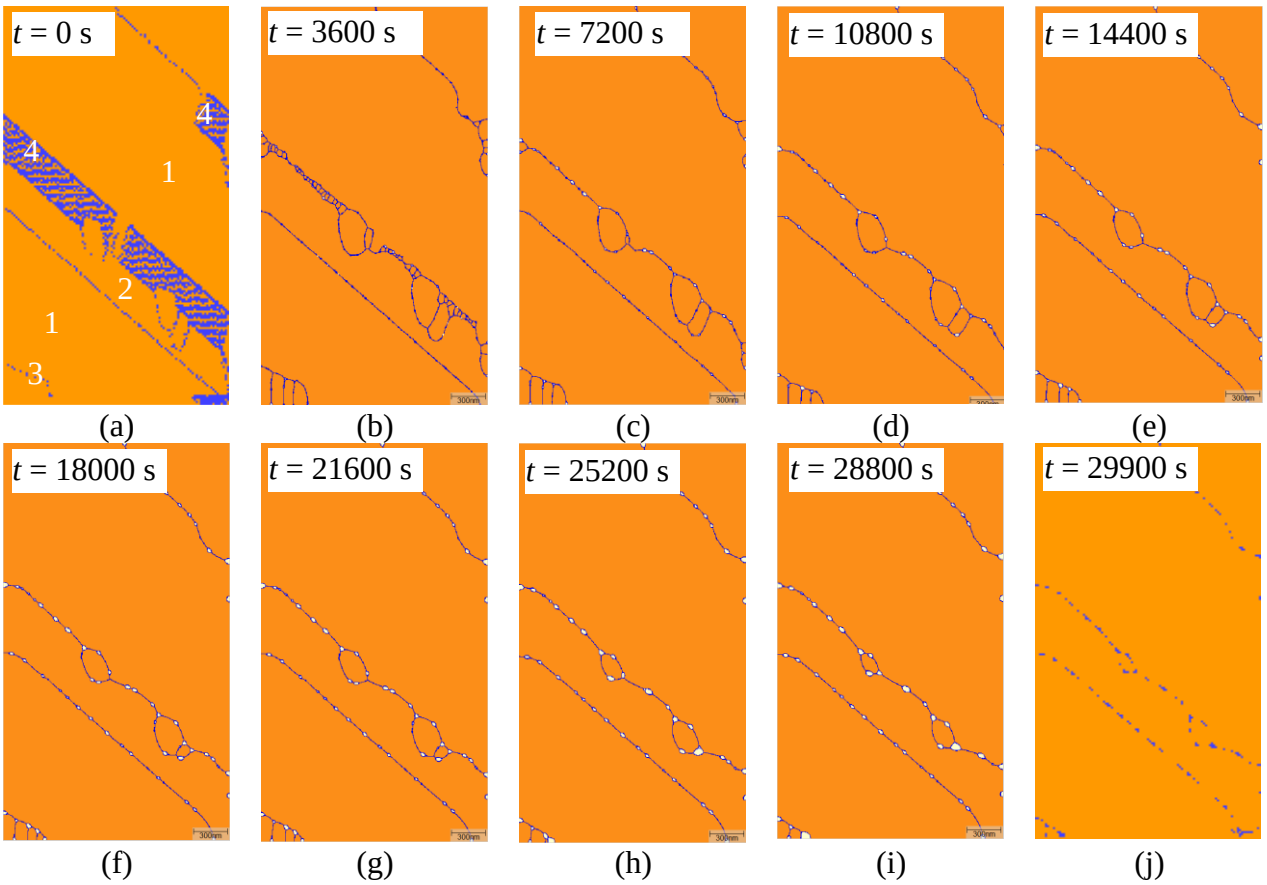

Fig. 3: (a)-(i) Displacement of the grain boundaries and growth of the β-phase within an time frame of 28800 s at an annealing temperature of 1023 K. (j) Subsequently, the temperature was reduced by quenching to RT with $\dot{T}$ = 0.7 K/s. At 293 K only the α-phase was displayed since the size of the β-phase grains was smaller than the numerical grid size.

Investigations at an annealing temperature of 1143 K were carried out for two different annealing times (2 and 4 hours) and two final quenching rates ($\dot{T}$ = 0.7 and 0.18 K/s). Note that the first quenching rate represents “air cooling” whereas the second represents “furnace cooling”. At the selected temperature the β-phase overgrows (see Fig. 4) most of the quaternary grains (labeled with 4). The β-grains formed a coherent region at the former grain boundaries. This indicates that nearly all quaternary grains were annihilated after 2 hours annealing time. The grains of the β-phase broadened during further annealing (Fig. 4c-d and f-g), while the width of the primary and secondary grains (labeled with 1 and 2) showed no grain boundary movement. Parts of the ternary grains (labeled with 3) have been overgrown by β−Ti, but not completely. After cooling down with only $\dot{T}$ = 0.18 K/s, the size of the β-Ti-grains were smaller than the numerical grid size and are thus located within the numerical grain boundaries (see Fig. 4e). The same happens after 4 hours annealing time and a quenching rate of $\dot{T}$ = 0.7 K/s (see Fig. 4h).

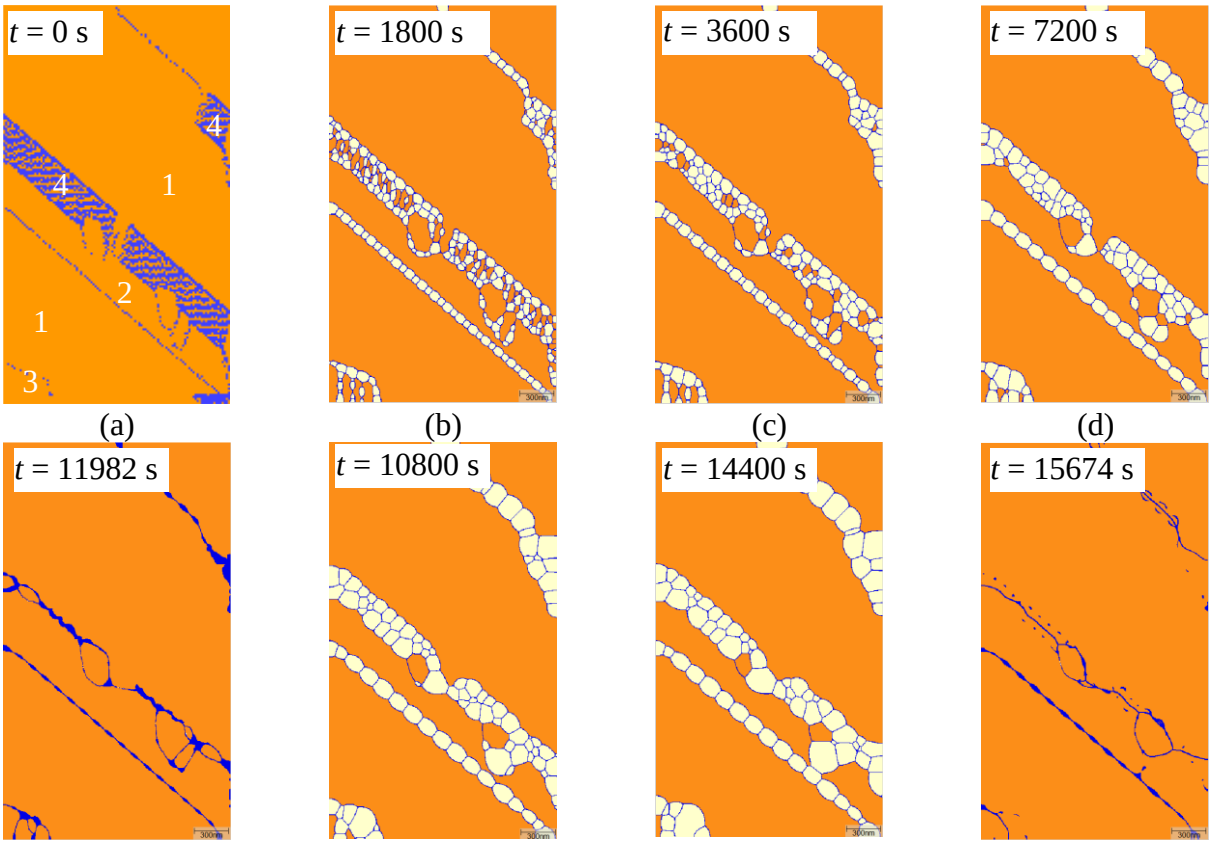

Fig. 4: Evolution of microstructures during aging heat treatment at an annealing temperature of 1143 K (a-d). The images show the first 2 hours of annealing. (e) The final microstructure after cooling down to RT with $\dot{T}$ = 0.18 K/s. (a-d) and (f-g) shows the microstructures for an heat treatment of 4 hours and (h) the microstructure at 293 K after quenching with $\dot{T}$ = 0.7 K/s.

In the second part of this section, the changes in the concentration distribution were examined. Investigations at an annealing temperature of 1023 K exhibited a shift of concentration at the phase boundaries. The change in the concentration distribution within the domain is shown in Fig. 5. At the beginning, the concentration is evenly distributed with 6 wt.% Al and 4 wt.% V (Fig. 5a). During the heat treatment a local concentration shift at the region around the grain boundaries was predicted. The concentration of Al increased in the surrounding of the newly formed β-phase while the concentration of V decreased. The change in concentration for Al is approximately 15 nm in the periphery of the new formed β-phase. In contrast, the concentration distribution for V changes over a larger distance and extends from the β-phase approximately 50-100 nm into the α-phase (see different dark blue and red color shades in Fig. 5b-c). Fig. 5d shows the final concentration distribution within the Ti-6Al-4V alloy. Due to the quenching process, no further alteration in the concentration dispersion compare to Fig. 5c occur.

Similar changes in the concentration distributions were also observed at an annealing temperature of 1143 K. First, we discuss the changes in the concentration pattern for an annealing time of 2 hours and a quenching rate of $\dot{T}$ = 0.18 K/s (Fig. 6). The amount of Al increase in the α-phase from 6 wt.% to 7.5 wt.% at the α/β-phase interface boundaries. The range of concentration shift was in an interval of about 10 nm around the β-phase. Outside these regions, the Al concentration is still uniform. Within the β-phase the Al concentration was between 5.5 wt.% and 5.7 wt.%. The concentration distribution of V differs considerably compare to Al. In the area of the α-phase, the concentration dropped from 4 wt.% to below 3.2 wt.% within a length of more than 200 nm and increased in the β-phase to more than 9.2 wt.% (Fig. 6a-c). This is understandable because the diffusion rate of

V in Ti is significantly higher compare to Al. It should be noted that the concentration pattern in the individual α grains is different. The larger the grain, the higher the V concentration in the middle since the concentration is balanced by diffusion. After cooling down to RT with $\dot{T}$ = 0.18 K/s, the V concentration reached a local concentration of over 42 wt.% within the grain boundaries (Fig. 6d).

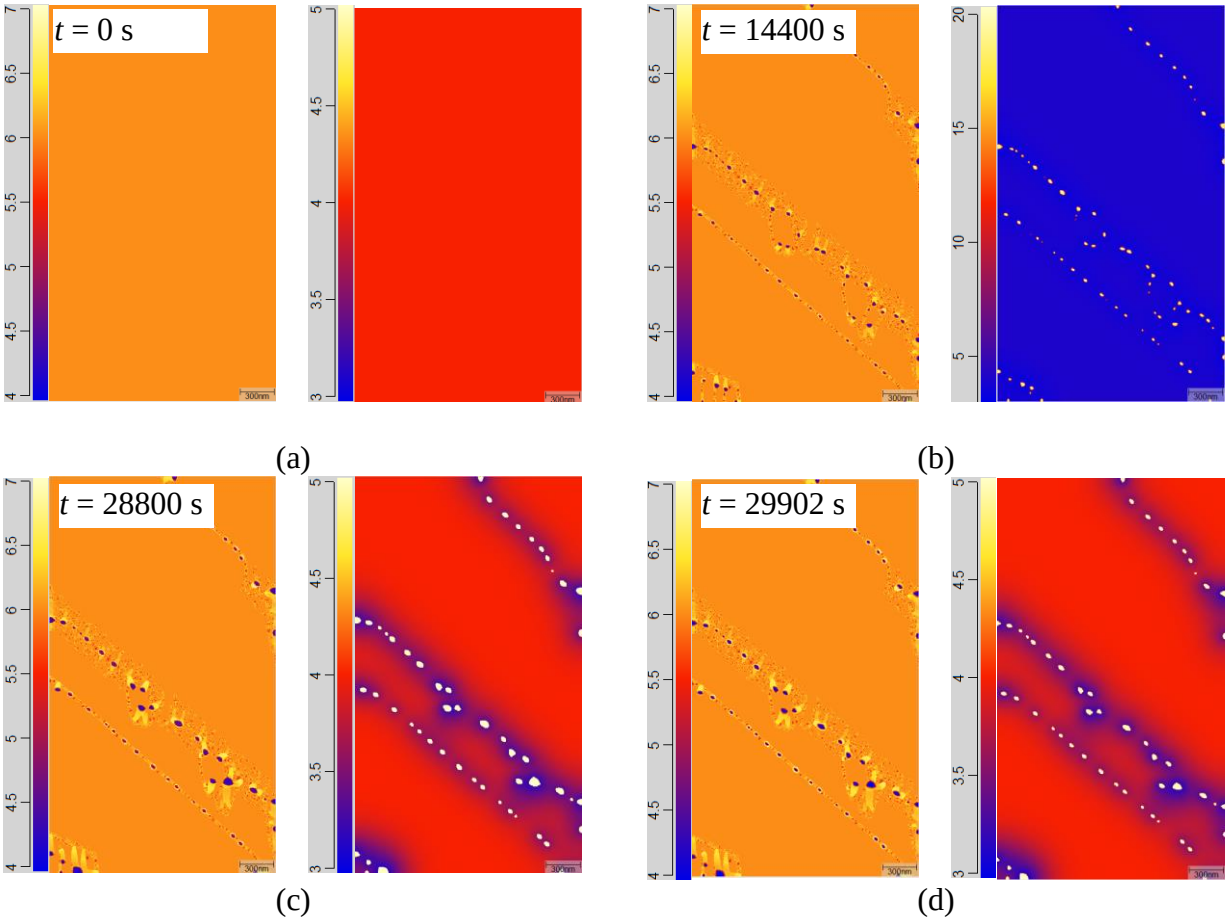

Fig. 5: (a)-(c) Evolution of concentration distributions of Al (left images) and V (right images) within 8 hours with an annealing temperature of 1023 K and (d) final concentration distribution after quenching to RT with $\dot{T}$ = 0.7 K/s.

In comparison, the alteration in the concentration pattern for an annealing time at 1143 K for 4 hours and a quenching rate to RT of $\dot{T}$ = 0.7 K/s is shown in Fig. 7. The first 2 hours correspond to the concentration spreading as given in Fig. 6a-c. The annealing time was now two times longer (4 hours) and only moderation concentration shifting was detected after the first 2 hours. The concentration of Al in the α-phase continues to be in the range of approximately 6 wt.% and the concentration increased within β-Ti from 5.5 wt.% after 2 additional hours to max. 5.82 wt.%. V reached a concentration distribution of 2.2 wt.% to 3 wt.% within the α-phase and 8.7 wt.% to 9.0 wt.% in the β-phase (Fig. 7a). After quenching, the local concentration of Al within the former β-phase area dropped down to 3.9 wt.%. In return, the concentration of V in these regions rose to over 30 wt.% (see Fig. 7b).

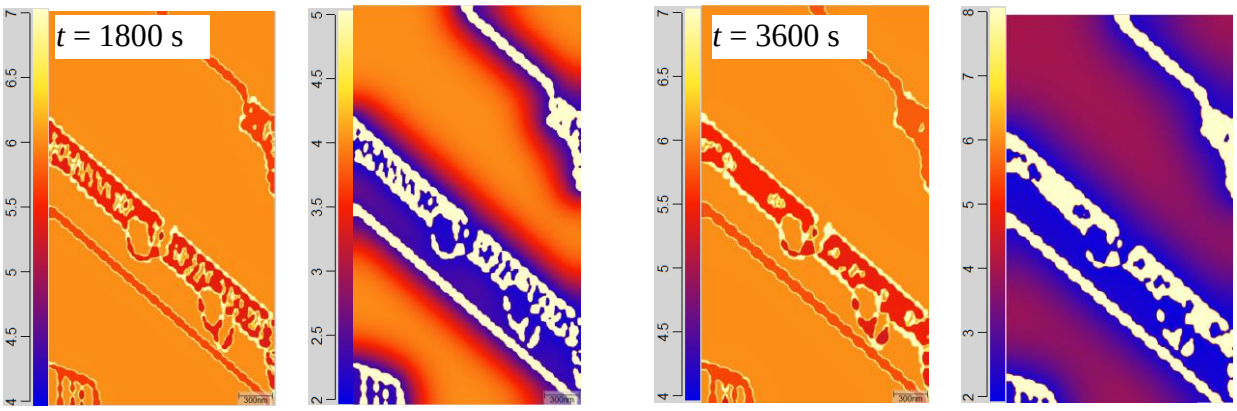

(a) (b)

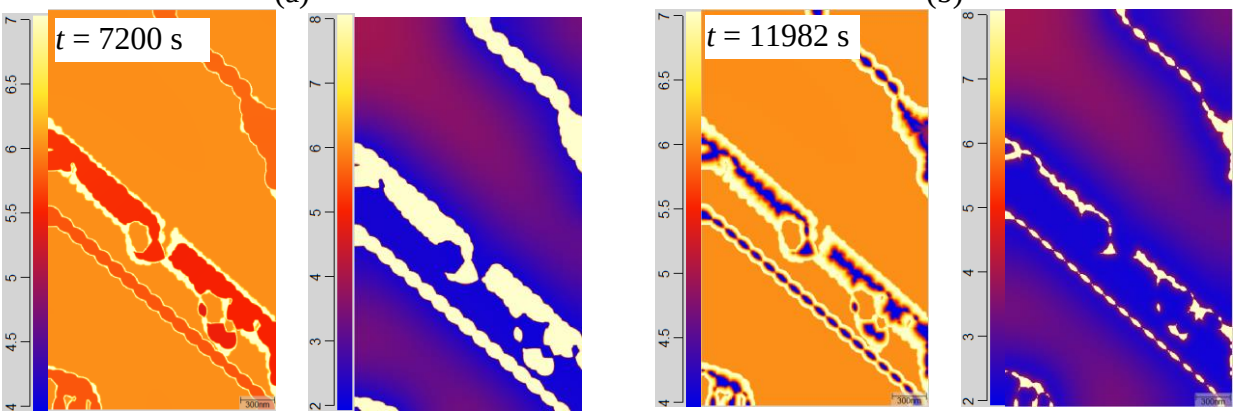

(c) (d)

Fig. 6: (a)-(c) Evolution of concentration distributions of Al (left images) and V (right images) within 2 hours for an annealing temperature of 1143 K and (d) final concentration distribution after cooling down to RT with $\dot{T}$ = 0.18 K/s.

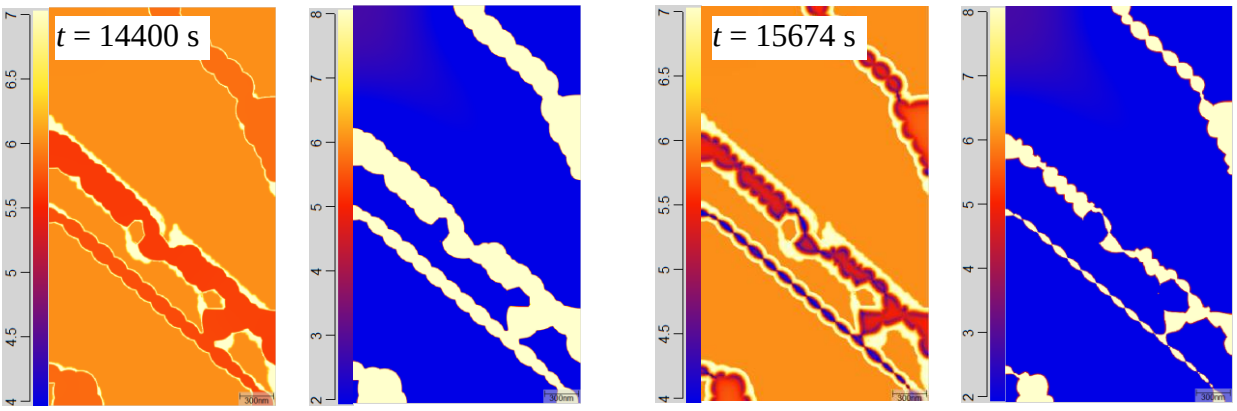

(a) (b)

Fig. 7: Evolution of concentration distributions of Al (left images) and V (right images) during heat treatment at an annealing temperature of 1143 K. (a) shows the last 2 hours of annealing and (b) the final distributions after cooling down to RT with $\dot{T}$ = 0.7 K/s.

Finally, the amount of the phase fraction was analyzed (Fig. 8). All results in common is the fact that the amount of the β-phase increased continuously and disappeared mostly during quenching. By comparing the equilibrium phase fractions according to Thermo-Calc with the ones obtained using our phase field investigations, it can be seen that the phase field simulation obtained a significant lower β-phase amount. Assuming global equilibrium, the phase fraction of β-Ti at 1023 K was calculated to be 0.7 (Fig. 1) and with phase field we got 0.01 (Fig. 8a). The situation is similar at an annealing temperature of 1243 K with a calculated equilibrium β-phase fraction of 0.38 compare to

0.2 obtained by phase field. Two reasons for this discrepancy are conceivable. First, the predefined "as-built" microstructure might not be fine enough. Although relatively small numerical cells were considered (5x5 nm^2), the resolved numbers of grain boundaries might be insufficient. Therefore, β-nucleation can be underpredicted. Second, the finite diffusivity of Al and V in the α-grains is restricting the growth of β. Equilibrium thermodynamic can, of course, not account for this effect

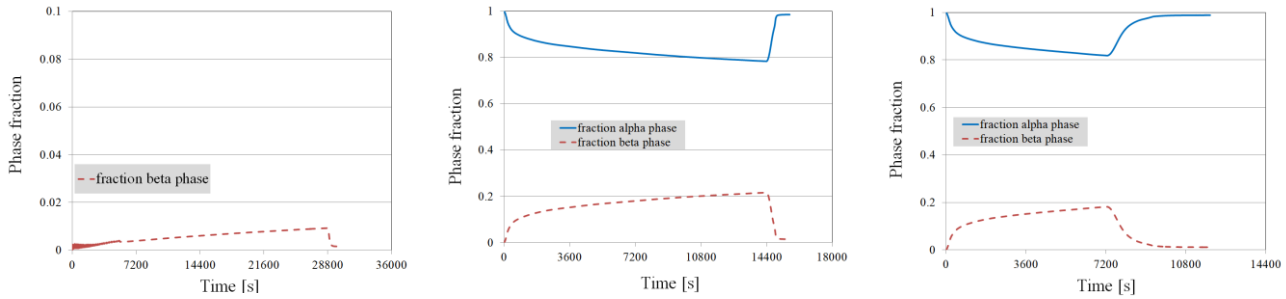

(a) (b) (c)

Fig. 8: Evolution of phase fraction for a heat treatment at 1023 K (a), and at 1243 K applying a high (b) and a low quenching rate (c).

Summary

The microstructure evolution during heat treatment of a Ti-6Al-4V alloy was numerical investigated. The task was carried out by using a phase-field based software code. Starting with a predefined "as built" microstructure that consists of four classes of martensitic α`-grains that typically occur after SLM production and assume that the thermodynamics of α and α` are similar, we have estimated the evolution of grain sizes and shapes, amount of phases, and corresponding concentration distributions during phase transition induced by annealing. Two annealing temperatures were selected, both below the critical temperature and the β-transus temperature. The annealing time for 1023 K was set to 8 hours and for the temperature of 1143 K to 2 and 4 hours, respectively. The associated quenching rates were $\dot{T}$ = 0.7 K/s and 0.18 K/s. The thermodynamic data were taken from the COST2 database and the diffusion values from different publications. The microstructure was specified to investigate the behavior of four different initial α`-grain sizes. It was found that for 1143 K the quaternary grains were overgrown by β in the first hour. Diffusion of Al led to a shift in concentration around the β-phase. In an environment of approximately 10 nm, the Al concentration rises above 6 wt.% and was depleted within the β-phase. For an annealing temperature of 1023 K, the quaternary α` grains either degenerate or were overgrown β. The ternary grains joined at a temperature of 1023 K and disappeared almost completely at 1143 K. During final cooling down to RT β-Ti fragmented, whereby the concentration distribution remains almost unchanged due to the high quenching rate. Therefore, the grain boundaries are enriched with V after the heat treatment.

REFERENCES

[1] W. Xu, E.W. Lui, A. Pateras, M. Qian, M.; Brandt, Acta Materialia 125, (2017), p.390.
[2] H.L. Du, P.K. Datta, J. . Burnell-Gray and D.B. Lewis, J. Mater. Sci. 30, (1995), p.2640.
[3] R.R. Boyer, Mater. Sci. Eng. A 213, (1996), p.103
[4] E.O. Ezugwu and Z.M. Wang, J. Mater. Process. Technol.68, (1997), p.262.
[5] C. Leyens and M. Peters, *Titanium and titanium alloys*, Wiley Online Library, (2003).
[6] S.L. Lu, M. Qian, H.P. Tang, M. Yan, J.Wang, D.H. StJohn, Acta Mater. 104, (2016**)**, p.303.
[7] Y. Ji,; T.W. Heo, F. Zhang, L.Q. Chen, J. Phase Equilib. Diffus. 37, (2016**)**, p. 53.
[8] C. Katinas, S. Liu, Y.C. Shin, J. Manuf. Sci. Eng., 141 (1) (2018) 011001.

[9] S. Liu, Y.C. Shin, Mater. Des. 159, (2018), pp. 212-223
[10] W.J. Evans, Mater. Sci. Eng. A 243, (1998), p.89.
[11] G.M. Ter Haar and T.H. Becker, Materials 11, (2018), p.146.
[12] https://micress.de
[13] European Commission and technical research, COST European cooperation in the field of scientific (1998) **2**: ISBN 92-828-3902-8.
[14] W.W. Xu, S.L. Shang, B.C. Zhou, Y. Wang, L.J. Chen, C. . Wang, X.J. Liu and Z.K. Liuc , Phys. Chem. Chem. Phys. 18, (2016), p.16870.
[15] Y. Mishin and C. Herzig, Acta Mater. 48, (2000), p.589.
[16] S.L. Shang, L.G. Hector, Y. Wang and Z.K. Liu, Phys. Rev. B: Condens. Matter Mater. Phys., 83, (2011), 224104.
[17] G. Lindwall, K.W. Moon, Z. Chen, M. Mengason, M.E. Williams, J.M. Gorham, J.C. Zhao and C.E. Campbell, J. Phase Equilib. Diffus. 39, (2018), p.731.
[18] https://www.thermocalc.com/products-services/databases/the-calphad-methodology/
[19] L. Scotti and A. Mottura, J. Chem. Phys. 142, (2015), 204308.
[20] L.L. Araùjo and M. Behar, Appl. Phys. A 71, (2000), p.169.
[21] S.Y. Lee, O. Taguchi and Y. Iijima, Materials Transactions, Vol. 51, No. 10, (2010), p.1809.
[22] S.L. Semiatin, S.L. Knisley, P.N. Fagin, F. Zhang, and D.R. Barker, Metallurgical and materials transactions A, 34, (2003), p.2377.